Cardiac Sympathetic PET Imaging with *meta*-[^{18}F]Fluorobenzylguanidine is Sensitive to Uptake-1 in Rats

Uzair S. Ismailani,[1,2] Ariel Buchler,[2,3] Gedaliah Farber,[1,2] Aleksandra Pekošak,[4] Eadan Farber,[2] Nicole MacMullin,[2] Erik J. Suuronen,[2] Neil Vasdev,[5] Rob S.B. Beanlands,[2] Robert A. deKemp,[2] and Benjamin H. Rotstein[1,2,3]*

[1] *Department of Biochemistry, Microbiology and Immunology, University of Ottawa, 451 Smyth Road, Ottawa, Ontario, K1H 8M5, Canada*

[2] *University of Ottawa Heart Institute, 40 Ruskin Street, Ottawa, Ontario, K1Y 4W7, Canada*

[3] *Department of Chemistry and Biomolecular Sciences, University of Ottawa, 10 Marie-Curie Private, Ottawa, Ontario, K1N 6N5, Canada*

[4] *VU Medical Centre, De Boelelaan 1085c, 1081 HV Amsterdam, Netherlands*

[5] *Azrieli Centre for Neuro-Radiochemistry, Centre for Addiction and Mental Health, 250 College Street, Toronto, Ontario, M5T 1R8, Canada*

Correspondence: Benjamin H. Rotstein, PhD
University of Ottawa Heart Institute
40 Ruskin Street, H-5219
Ottawa, Ontario, Canada
K1Y 4W7
Phone: 613-696-7324
Email: benjamin.rotstein@uottawa.ca

Abstract

Dysfunction of the cardiac sympathetic nervous system contributes to the development of cardiovascular diseases including ischemia, heart failure, and arrhythmias. Molecular imaging probes such as *meta*-[^{123}I]iodobenzylguanidine have demonstrated the utility of assessing neuronal integrity by targeting norepinephrine transporter (NET, uptake-1). However, current radiotracers can report only on innervation due to suboptimal kinetics and lack of sensitivity to NET in rodents, precluding mechanistic studies in these species. The objective of this work was to characterize myocardial sympathetic neuronal uptake mechanisms and kinetics of the positron emission tomography (PET) radiotracer *meta*-[^{18}F]fluorobenzylguanidine ([^{18}F]mFBG) in rats. Automated synthesis using spirocyclic iodonium(III) ylide radiofluorination produces [^{18}F]mFBG in 24% ± 1% isolated radiochemical yield and 30–95 GBq/μmol molar activity. PET imaging in healthy rats delineated the left ventricle, with mono-exponential washout kinetics (k_{mono} = 0.027 ± 0.0026 min^{-1}, A_{mono} = 3.08 ± 0.33 SUV). *Ex vivo* biodistribution studies revealed tracer retention in the myocardium, while pharmacological treatment with selective NET inhibitor desipramine, non-selective neuronal and extraneuronal uptake-2 inhibitor phenoxybenzamine, and neuronal ablation with neurotoxin 6-hydroxydopamine reduced myocardial retention by 33%, 76%, and 36%, respectively. Clearance of [^{18}F]mFBG from the myocardium was unaffected by treatment with uptake-1 and uptake-2 inhibitors following peak myocardial activity. These results suggest that myocardial distribution of [^{18}F]mFBG in rats is dependent on both NET and extraneuronal transporters and that limited reuptake to the myocardium occurs. [^{18}F]mFBG may therefore prove useful for imaging intraneuronal dysfunction in small animals.

Keywords: norepinephrine transporter; sympathetic nervous system; cardiac imaging; *meta*-[^{18}F]fluorobenzylguanidine; positron emission tomography; fluorine-18

Introduction

The autonomic nervous system (ANS) has a crucial role in governing cardiac homeostasis, and in regulating functions including heart rate, blood pressure, and contractility.[1] The sympathetic branch of the ANS supplies excitatory stimuli to increase such functions above basal levels through the release of norepinephrine (NE) as the major postganglionic neurotransmitter, whereas the parasympathetic branch produces opposing effects using acetylcholine (ACh).[1,2] Loss of autonomic regulation in favour of increased sympathetic activity and vagal withdrawal has been described in chronic heart failure, cardiac arrythmias, sudden cardiac death, and diabetes mellitus.[3–6] As such, sympathetic dysfunction is considered central to many pathologies, and molecular imaging is used clinically for both mechanistic investigations and risk stratification in cardiovascular disease.[2,7–11]

Currently available radiotracers used for nuclear imaging of cardiac sympathetic dysfunction predominantly target the norepinephrine transporter (NET) to detect defects in global and regional myocardial presynaptic nerve density.[12] Radiolabeled neurotransmitters such as [^{11}C]epinephrine, [^{11}C]norepinephrine, [^{11}C]phenylephrine, and fluorinated dopamine derivatives can be imaged by positron emission tomography (PET) and exhibit high selectivity and rapid uptake by NET, but are complicated by both peripheral and intraneuronal metabolism giving rise to multiple substrates with distinct kinetics and target affinities.[13] These challenges were overcome with the development of structural analogs lacking catechol functionality such as the substituted amphetamine derivative *meta*-[^{11}C]hydroxyephedrine ([^{11}C]HED), and benzylguanidines *meta*-[^{123}I]iodobenzylguanidine ([^{123}I]mIBG, used for lower resolution single-photon emission computed tomography or planar scintigraphy) and [^{18}F]flubrobenguane ([^{18}F]FBBG, formerly [^{18}F]LMI1195, Figure 1).[14] While NET-mediated neuronal retention provides excellent cardiac

imaging contrast for these analogues, rapid uptake kinetics hinder the accurate quantification of sympathetic nerve abnormalities and cannot report on neural tone, thus necessitating the continued development of sympathetic nervous system (SNS) radiotracers which are easily accessible and possess favourable myocardial kinetics.[15–18] To this end, another benzylguanidine, *meta*-(3-[^{18}F]fluoropropyl)benzylguanidine ([^{18}F]mFPBG), has been developed for more facile alkyl radiofluorination and has shown utility for neuroblastoma imaging and preclinical cardiac imaging.[19]

More recently, radiotracer candidates bearing a phenethylguanidine core (Figure 1) have exhibited slower neuronal uptake rates in human imaging while maintaining irreversible kinetics due to vesicular trapping mediated by vesicular monoamine transporter 2 (VMAT2).[20] Initial challenges associated with nucleophilic ^{18}F-fluorination of the electron-rich aromatic rings in 4-[^{18}F]fluoro-*meta*-hydroxyphenethylguanidine ([^{18}F]4F-MHPG) have since been overcome using spirocyclic iodonium ylide radiofluorination.[16,21,22] Nevertheless, [^{18}F]4F-MHPG and its isomer [^{18}F]3F-PHPG inspired the development of [^{18}F]AF78, which retains the phenethylguanidine core with an appended 3-fluoropropyl ether moiety for more facile radiolabeling.[23] Preliminary studies with [^{18}F]AF78 have demonstrated cardiac retention in rats likely due to extraneuronal uptake mechanisms. However, further *in vivo* evaluation of this tracer is required to assess NET-dependent uptake in rats and higher species.

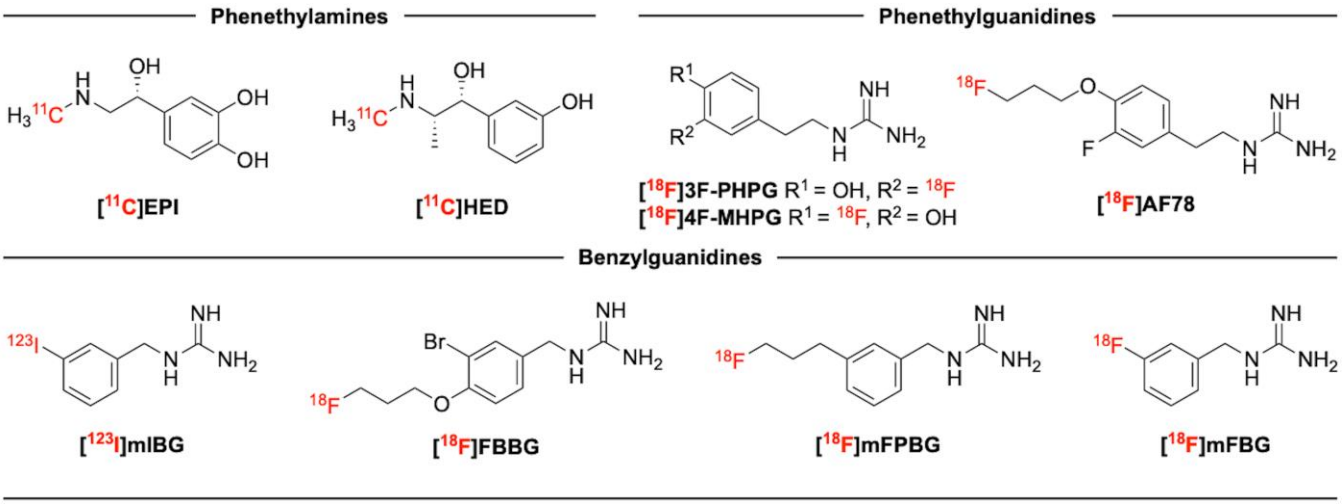

Figure 1. Chemical structures of norepinephrine radiotracer mimics used for SNS imaging.

meta-[^{18}F]Fluorobenzylguanidine ([^{18}F]mFBG) is the closest structural analogue of [^{123}I]mIBG that can be used for imaging with fluorine-18 ($t_{1/2}$ = 109.7 min), the most convenient PET nuclide for labeling, transport, and dynamic imaging of small molecules. [^{18}F]mFBG was first reported in the 1990s but has not since been evaluated for cardiac SNS imaging.[24] While analogous to [^{123}I]mIBG, and to some extent [^{18}F]FBBG, available evidence suggests that [^{18}F]mFBG possesses lower affinity for NET, as well as reduced lipophilicity and serum protein binding.[25] Given these attributes, [^{18}F]mFBG may exhibit slower uptake into tissue, with distribution less dependent on tissue perfusion. This hypothesis is consistent with observable myocardial washout in [^{18}F]mFBG human imaging,[26] in contrast to the very slow washout kinetics that [^{123}I]mIBG displays,[27,28] and irreversible cardiac uptake of [^{11}C]HED and [^{18}F]FBBG.[29] We were further attracted to [^{18}F]mFBG by its potential for faster myocardial clearance and slower reuptake as it may provide critical information on sympathetic tone and improvements in quantification of neuronal dysfunction.[29]

However, due to synthetic challenges associated with radiofluorination of deactivated arenes, the development of this compound has been gradual, with few recent reports demonstrating the utility of [^{18}F]mFBG for imaging neuroendocrine tumors.[26,30] New syntheses have been reported using either copper-mediated radiofluorination or diaryliodonium salt precursors, both of which are accompanied by technical challenges related to automation and access to precursors.[26,31–34] In addition, [^{18}F]mFBG is often obtained using biocompatible HPLC eluent, resulting in dilute activity concentrations that present an obstacle for routine production and small animal imaging studies. Using our previously reported methodology, we sought to develop an improved practical synthesis of [^{18}F]mFBG by spirocyclic iodonium ylide (SCIDY) radiofluorination.[35] The SCIDY precursor is prepared in three steps from commercially available reagents, radiolabeled, and subsequently reformulated using a carboxymethyl (CM) ion exchange resin to obtain the tracer in activity concentrations >370 MBq/mL, suitable for transport and imaging. The enhanced accessibility of this radiotracer prompted us to evaluate its pharmacokinetic properties and utility for cardiac SNS imaging in Sprague Dawley (SD) rats. Our *in vivo* and *ex vivo* evaluation includes PET imaging to assess tissue contrast and myocardial kinetics, metabolite analysis to gauge tracer stability, biodistribution to determine tracer localization, pharmacological blocking studies using desipramine (DMI) and phenoxybenzamine (PBZ), and chemical sympathectomy with 6-hydroxydopamine (6-OHDA) to study tracer uptake mechanisms.

Results and Discussion

Automated radiosynthesis of [^{18}F]mFBG in high activity yields. The synthetic route to obtain the precursor was first described by Rotstein *et al.*[35] Briefly, synthesis of the radiolabeling precursor began by guanylation of *meta*-iodobenzylamine to form the partially protected *meta*-

iodobenzylguanidine **1** in 56% yield (Scheme 1). Following complete protection to afford compound **2** (92%), the intermediate was oxidized using Selectfluor and trimethylsilyl acetate,[36] followed by the addition of spiroadamantyl-1,3-dioxane-4,6-dione (SPIAd, **3**) to obtain the SCIDY precursor **4** in 54% yield (Scheme 1). Precursor stability studies conducted by NMR spectroscopy only revealed decomposition of the ylide after >6 months when stored at ambient temperature, but no apparent degradation upon long term storage at lower temperatures (<6 °C, Table S1).

Scheme 1. Synthetic route to prepare the SCIDY precursor.

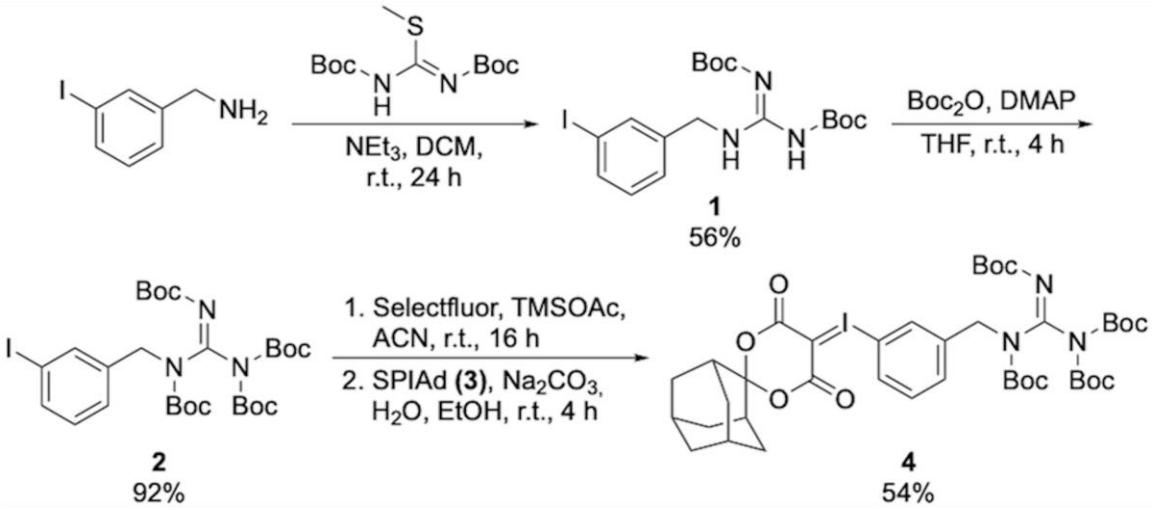

Further optimization of the previously reported radiolabeling conditions was carried out manually with low levels of starting radioactivity.[35] Radiochemical yields were determined by radioTLC integration of product peaks and unreacted [^{18}F]fluoride. This two-step radiosynthesis first incorporates [^{18}F]fluoride by nucleophilic substitution, followed by acidic deprotection (Scheme 2). Radiofluorination of **4** in the presence of tetraethylammonium bicarbonate (TEAB) in DMF afforded the desired intermediate [^{18}F]**5** in 42 ± 11% yield after 5 minutes (Figure 2A). In line with previous studies on SCIDY radiofluorination, prolonged reaction times or elevated base concentrations above the optimal range of 4–6 equiv. had deleterious effects on precursor stability

and radiochemical yield (RCY, Figure 2B).[22,35,37] Higher overall yields were observed in DMSO after 10 minutes (55 ± 9%) compared to DMF (Figure 2A), while replacing TEAB with potassium carbonate and Kryptofix® ($K_2CO_3/K_{2.2.2}$) led to markedly lower yields in either solvent (<7%, Table S2). Nearly quantitative disappearance of protected intermediate [^{18}F]**5** in the presence of 12 M HCl was observed after 5 minutes to form the desired product [^{18}F]**6** ([^{18}F]mFBG). Previously described radiofluorination reactions with iodonium ylides using Meldrum's acid as an auxiliary have suggested the formation of radiolabeled regioisomers as byproducts.[38] We prepared authentic standards of both *ortho*- and *para*-fluorobenzylguanidine and did not detect these radiochemical impurities from SCIDY radiofluorination (Figures S2-S3). In summary, [^{18}F]mFBG was formed with high selectivity, and synthesized in 53% RCY within 15 minutes.

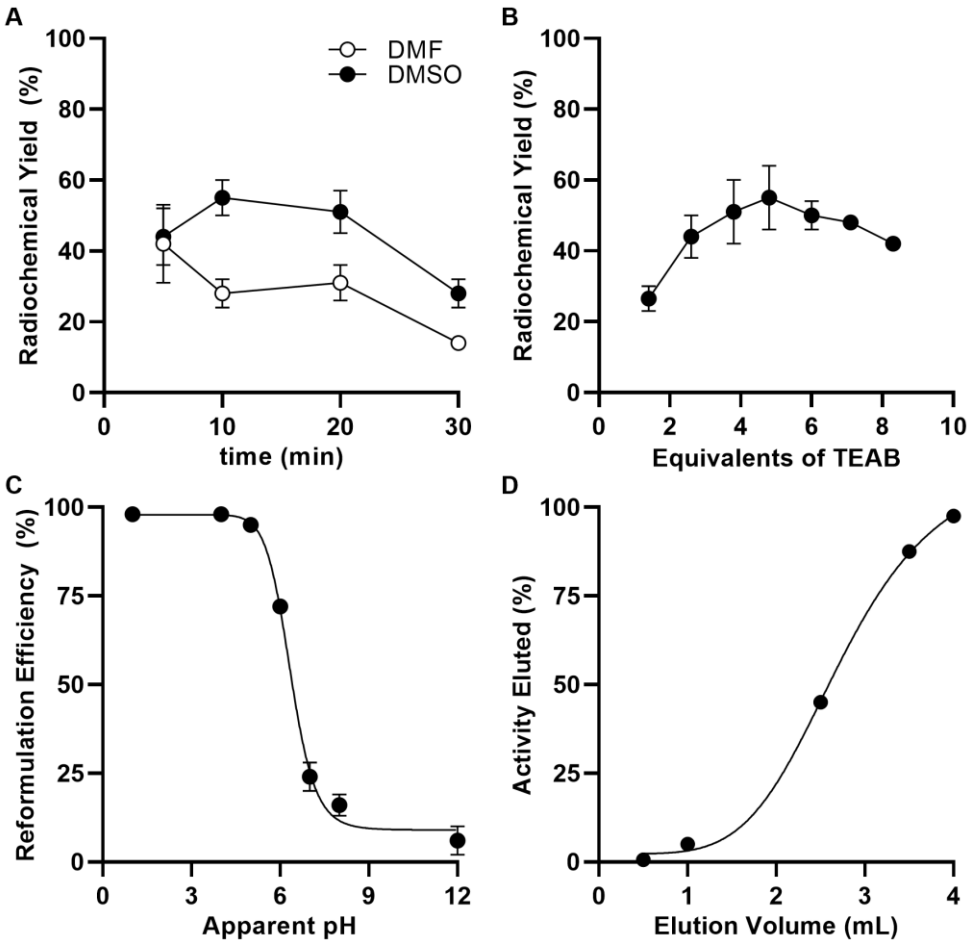

Figure 2. Optimization of [^{18}F]**5** radiofluorination and [^{18}F]mFBG reformulation conditions. Dependence on (A) solvent (n = 1–4), and (B) base concentration (n = 2–4). Conditions: 20 mM precursor, 200 µL DMSO, 10 min, 120 °C. Radiochemical yield of [^{18}F]**5** determined by radioTLC integration of product peaks and unreacted [^{18}F]fluoride. Product identity was confirmed by radioHPLC and co-injection of nonradioactive standard. (C) Dependence of [^{18}F]mFBG reformulation efficiency (RE) on influent pH (n = 6). RE is defined as the product of the trapping and elution efficiencies. (D) Volume of saline required for [^{18}F]mFBG elution (n = 6).

Using the optimized conditions, an automated two-step production of [^{18}F]mFBG was performed using the GE TRACERlab FX2N radiosynthesis module with in-line semi-preparative HPLC purification (Scheme 2, Figures S5-6). Following purification, we screened commercially available resins to concentrate the radiotracer. We observed no retention of [^{18}F]mFBG on commonly used C18 and HLB solid phase extraction cartridges. However, the weak ion-exchange

CM resin showed greater promise for trap and release reformulation during initial screening, enabling the isolation of [^{18}F]mFBG in high activity concentrations. Unsurprisingly, we noted a dependency of activity retained by the CM resin on the pH of the influent solution collected from semi-preparative HPLC purification (Figure 2C). At pH >7, we noted poor REs (<25%), while a mildly acidic pH resulted in a steep increase to 48 ± 4%. Nearly quantitative retention (98 ± 1%) was achieved at pH ≤5, followed by complete elution of [^{18}F]mFBG in a maximum of 4 mL of physiological saline in activity concentrations >370 MBq/mL (Figure 2D). Satisfied with the quality of our reformulation, the entire production was then automated to reliably obtain the radiotracer in 55–65 minutes from the beginning of synthesis, in an isolated decay corrected yield of 24% ± 1% and in high molar activity (30–95 GBq/µmol), suitable for our preclinical evaluation (Scheme 2).

Scheme 2. Automated radiosynthesis of [^{18}F]mFBG.

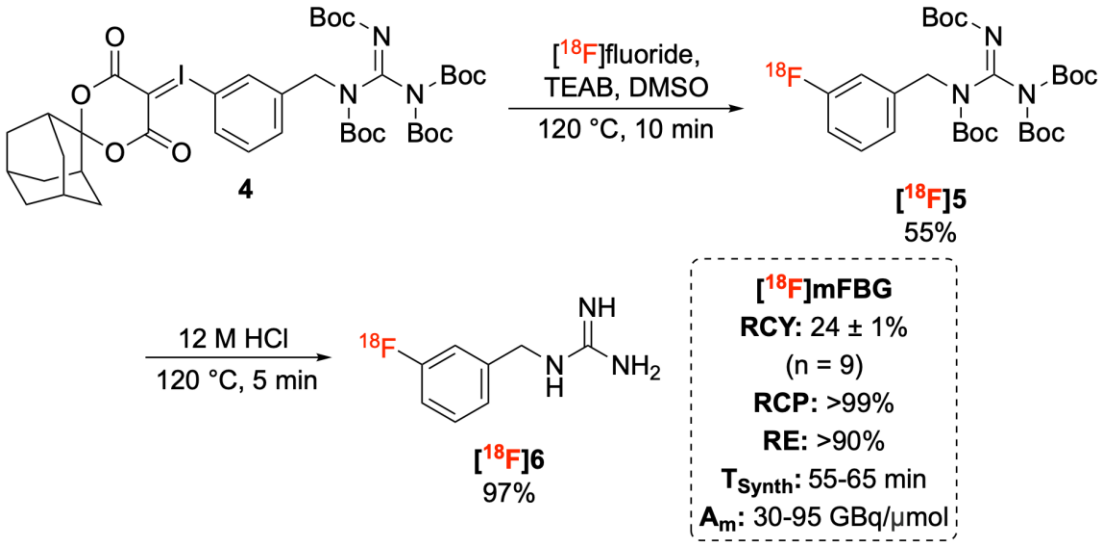

[^{18}F]mFBG exhibits cardiac uptake in SD rats. Dynamic PET scans were performed over 60 minutes to assess the cardiac imaging quality and myocardial kinetics of [^{18}F]mFBG in male SD

rats following intravenous injection of the tracer in the lateral tail vein (Figure 3). The images show uniform uptake in the left ventricle (LV) that peaks at >3.0 SUV from 2.5–5 minutes. Minimal bone uptake was observed and did not interfere with quantification of LV activity (Figures S8-S9). While liver uptake remained constant after 30 minutes (2.69 ± 0.04 SUV), cardiac activity decreased monoexponentially after peak uptake (r^2 = 0.93, 5–55 min), with an observed k_{mono} = 0.027 ± 0.0026 min^{-1} and A_{mono} = 3.08 ± 0.33 SUV. Increased LV clearance of [^{18}F]mFBG is likely due to its reduced NET affinity (as measured *in vitro*) and lipophilicity in comparison to other benzylguanidine radiotracers,[25] since [^{123}I]mIBG and [^{18}F]FBBG display slow washout or irreversible uptake in rat myocardium.[39] Structure-activity relationships of benzylguanidines with respect to NET are complex, though it has been appreciated that *meta*-bromo or -iodo substitution and *para*-hydroxy or -alkoxy substituents are associated with NET-mediated uptake.[40] In this context, the observed faster clearance of [^{18}F]mFBG compared to [^{123}I]mIBG and other reported analogues is in line with expectations and *in vitro* measurements. Considerable radiotracer washout from the myocardium over the course of a dynamic PET scan enables the use of readily available kinetic analyses such as k_{mono} and Logan plots for quantitative interpretation. Encouraged by the *in vivo* cardiac time-activity profiles, we next sought to better understand the mechanisms of [**^{18}**F]mFBG distribution.

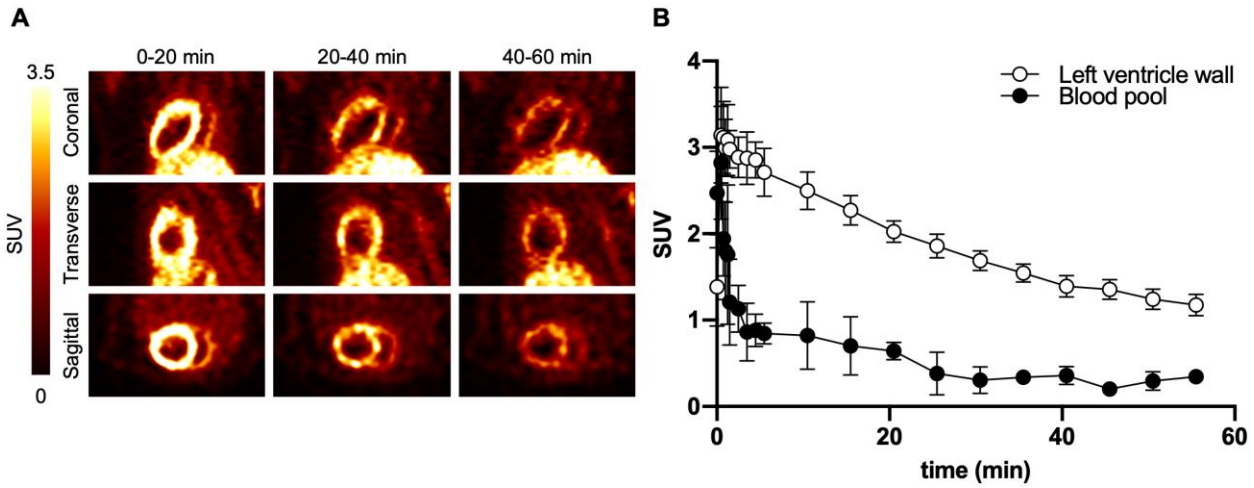

Figure 3. *In vivo* baseline PET imaging of the myocardium in SD rats. (A) Representative myocardial PET images and (B) corresponding time-activity curves (n = 5).

Ex vivo biodistribution studies were performed in male rats under baseline conditions at 30 minutes following intravenous radiotracer administration via the lateral tail vein, after blood pool activity stabilized (Table 2). As expected, high uptake in the myocardium was detected (3.12 ± 0.61 %ID/g) along with considerable distribution to other innervated organs such as the lung (1.12 ± 0.28 %ID/g), spleen (0.96 ± 0.22 %ID/g), adrenal gland (1.56 ± 0.36 %ID/g), and thyroid (1.25 ± 0.24 %ID/g). Renal retention (0.85 ± 0.03 %ID/g) predominated over hepatic retention (0.56 ± 0.27 %ID/g), and moderate bone uptake (0.85 ± 0.21 %ID/g) was observed in the femur, likely due to *in vivo* defluorination and consistent with previously reported findings on [^{18}F]mFBG and related benzylguanidines.[32,39] The heart to blood (H:B) ratio was found to be 13.12, similar to [^{123}I]mIBG and [^{18}F]FBBG, despite lower NET affinity discussed above.[39] We conducted the same experiment on female rats (Table 1), and observed comparable retention in all organs except for the kidney (0.63 ± 0.09 %ID/g, p = 0.035).

Table 1. *Ex vivo* biodistribution in SD rats at 30 minutes.

	%ID/g				
Organ	**Baseline uptake**		**Uptake-1 blockade**		**Uptake 1 + uptake 2 blockade**
	Male	Female	Vehicle	DMI	PBZ
Heart	3.12 ± 0.61	3.08 ± 0.59	3.45 ± 0.69	2.40 ± 0.23 *	0.85 ± 0.12 *
Liver	0.56 ± 0.27	0.90 ± 0.46	0.54 ± 0.28	0.88 ± 0.33	0.64 ± 0.16
Kidney	0.85 ± 0.03	0.63 ± 0.09 *	0.87 ± 0.05	0.72 ± 0.18	5.05 ± 0.49 *
Lung	1.12 ± 0.28	1.26 ± 0.14	1.07 ± 0.35	0.75 ± 0.16	1.18 ± 0.15
Blood	0.24 ± 0.02	0.24 ± 0.08	0.26 ± 0.03	0.18 ± 0.07 *	0.27 ± 0.03
Spleen	0.96 ± 0.22	1.03 ± 0.21	0.99 ± 0.25	0.44 ± 0.11 *	0.74 ± 0.10
Adrenal	1.56 ± 0.36	1.50 ± 0.16	1.59 ± 0.43	0.58 ± 0.37 *	0.12 ± 0.02 *
Thyroid	1.25 ± 0.24	1.77 ± 0.68	1.29 ± 0.27	1.31 ± 0.36	1.37 ± 0.16
Bone	0.85 ± 0.21	0.77 ± 0.07	0.89 ± 0.24	0.59 ± 0.36	0.79 ± 0.16
H:B	13.12 ± 0.61	13.50 ± 3.48	13.27 ± 2.43	14.24 ± 1.50	3.40 ± 0.24 *
Animal weight (g)	111 ± 6	107 ± 3	125 ± 8	111 ± 10	100 ± 1

* Statistical significance ($p < 0.05$) reached by unpaired t-test comparing sexes (male and female, $n = 4$), and vehicle ($n = 5$) to uptake-1 blockade (DMI 1 mg/kg, $n = 5$), and uptake-1 + uptake-2 blockade (PBZ 27 ± 3 mg/kg, $n = 3$).

[^{18}F]mFBG is intact in SD rat myocardium. Next, we assessed the *in vivo* stability of [^{18}F]mFBG at the 30-minute time-point in myocardium and plasma samples (Figure 4A). Activity from the myocardium was extracted by homogenization, and metabolites were separated using reversed-phase HPLC. Fractions were collected every minute and radioactivity was quantified using a gamma counter. The parent compound accounted for 98 ± 1% and 97 ± 1% of myocardial uptake, with extraction efficiencies of 76 ± 3%, and 78 ± 2%, for males and females, respectively. These findings are consistent with previous reports on related NET radioligands and demonstrate selective uptake and limited myocardial metabolism of the radiotracer.[18,41,42] Concurrently, [^{18}F]mFBG-associated activity was assessed in plasma following separation and protein precipitation of whole blood samples obtained via cardiac puncture. The parent fraction represented 22 ± 4 % and 20 ± 2% of total radioactivity with extraction efficiencies of 82 ± 2% and 81 ± 3% in males and females, respectively (Figure 4A). This is in marked contrast to the 90% parent fraction in plasma reported during human imaging experiments conducted by Pandit-Taskar *et al.*,[26] and likely arises from more aggressive peripheral metabolism in rodents. Lastly, we

investigated the stability of [^{18}F]mFBG in human serum (Figure 4B), incubated at 37 °C and aliquoted samples for HPLC analysis at 0, 15, 60, and 120 minutes. Up to a 2-hour incubation, the tracer was found to remain 99% intact.

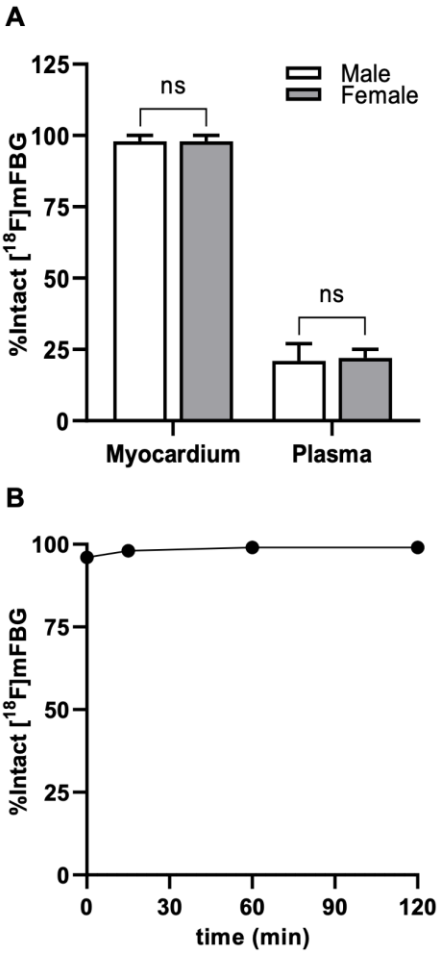

Figure 4. Percent intact [^{18}F]mFBG in (A) myocardium (n = 2), and plasma (n = 4) at 30 minutes *in vivo*, and (B) human serum *in vitro* (n = 1).

[^{18}F]mFBG uptake is dependent on uptake-1 and uptake-2 transporters. To determine the uptake mechanisms of this tracer, animals were pre-treated with vehicle, desipramine (DMI, 1 mg/kg, iv), or phenoxybenzamine (PBZ, 27 ± 3 mg/kg, iv) 10 minutes prior to [^{18}F]mFBG administration and sacrificed at the 30-minute time-point (Table 1). DMI has been extensively

evaluated in rodents and humans as a potent and selective NET inhibitor, while PBZ inhibits both neuronal and extraneuronal uptake non-selectively.[12,43–45] *Ex vivo* tissue counting experiments revealed 31% and 76% reductions in myocardial uptake with DMI (2.40 ± 0.23 %ID/g, $p = 0.01$), and PBZ (0.82 ± 0.12 %ID/g, $p < 0.0001$), respectively, in comparison to vehicle (3.45 ± 0.69 %ID/g). *In* vivo PET imaging recapitulated these findings (Figure 5A), and time-activity curves revealed an increase in k_{mono} (accelerated washout) following DMI pre-treatment (0.058 min^{-1} vs 0.020 min^{-1}, $p = 0.044$). Uptake-1 and uptake-2 blockade also significantly reduced tracer retention in the blood pool and other innervated organs (Table 1).

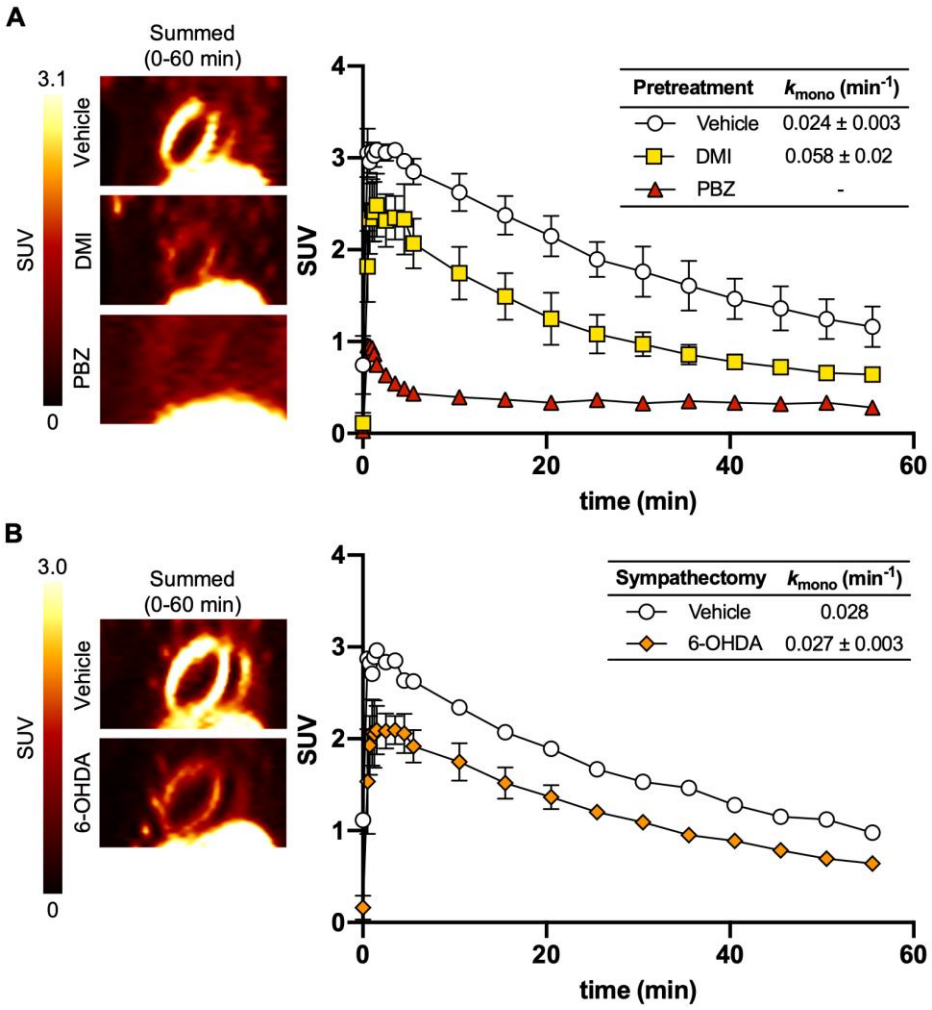

Figure 5. Representative *in vivo* myocardial PET imaging in SD rats following (A) pre-treatment (n = 1-3) and (B) chemical sympathectomy (n = 1-3).

To provide additional evidence for tracer uptake in cardiac sympathetic neurons, chemical sympathetic denervation using 6-OHDA was performed on rats following an established treatment cycle.[46–48] [^{18}F]mFBG was administered one week after the last 6-OHDA treatment, and organ uptake was measured *ex vivo* (Table 2). Myocardial tracer retention was reduced by 36% (1.32 ± 0.27 %ID/g, p = 0.02) relative to vehicle controls (2.04 ± 0.07 %ID/g). Notably, 6-OHDA treatment also reduced uptake in the spleen (0.30 ± 0.04, p <0.0001), and lowered the H:B ratio to 11.11 ± 2.21 compared to 17.20 ± 2.22 in vehicle treated rats (p = 0.01). The magnitude of the

observed reduction of myocardial uptake with 6-OHDA treatment is consistent with the results obtained from DMI blocking experiments, indicating that [^{18}F]mFBG localizes within myocardial sympathetic neurons, mediated by NET. Representative PET images and time-activity curves for this treatment group further illustrate reduced LV myocardial uptake, with k_{mono} values remaining unaffected (Figure 5B).

We also performed autoradiography on mid-ventricular myocardial sections prepared from the same cohort of vehicle, PBZ, and 6-OHDA-treated rats (Figure 6). Comparable results were obtained by *ex vivo* autoradiography experiments, displaying high uptake of [^{18}F]mFBG throughout the LV (14.3 ±1.9 %ID×kg/m^2), in comparison to those pre-treated with PBZ (3.49 ± 0.99 %ID×kg/m^2, p = 0.02). Similarly, reduced uptake was observed in animals treated with 6-OHDA (8.07 ± 0.54 %ID×kg/m^2, p = 0.04) in comparison to vehicle controls (15.47 ± 2.10 %ID×kg/m^2). The uptake in the LV was observed to be homogenous in all samples. A reduction in myocardial uptake (Table 2) was also noted in rats treated with vehicle in comparison to our previously established baseline (Table 1) when measured in units of %ID/g. Myocardial sympathetic innervation is known to decrease in Wistar rats over one year in age,[49] and it is possible that a similar phenomenon could occur in young Sprague-Dawley animals. However, the apparent difference was resolved when expressing the dataset as standard uptake values (SUV, Table S3), suggesting that variations in animal bodyweight associated with the prolonged treatment cycle were responsible for this change.

Table 2. *Ex vivo* biodistribution in 6-OHDA treated SD rats at 30 minutes.

	%ID/g		
Organ	**Vehicle**	**6-OHDA**	
Heart	2.04 ± 0.07	1.32 ± 0.27	*
Liver	1.50 ± 0.23	1.49 ± 0.13	
Kidney	0.63 ± 0.13	0.73 ± 0.12	
Lung	1.30 ± 0.15	1.25 ± 0.29	
Blood	0.12 ± 0.02	0.12 ± 0.00	
Spleen	1.08 ± 0.10	0.30 ± 0.04	*
Adrenal	1.62 ± 0.29	1.41 ± 0.44	
Thyroid	1.56 ± 0.36	1.38 ± 0.35	
Bone	0.77 ± 0.25	1.01 ± 0.22	
H:B	17.20 ± 2.22	11.11 ± 2.21	*
Animal weight (g)	240 ± 12	235 ± 28	

* Statistical significance ($p < 0.05$) reached by unpaired t-test ($n = 4$).

NET blockade with DMI in rats has previously been shown to reduce radiotracer uptake in the myocardium using [^{11}C]HED and [^{18}F]mFPBG, but not [^{123}I]mIBG and [^{18}F]FBBG, due to a dominant contribution of extraneuronal uptake-2 dependent catecholamine handling of these latter molecules.[50–52] Consequently, NET-selective uptake with previously studied benzylguanidines is typically observed only in rabbits and higher species, where myocardial tracer retention is reduced by >60%.[53] Based on our findings, neuronal and extraneuronal uptake in the rat myocardium account for 31–36%, and 40–45% of [^{18}F]mFBG signal, respectively.

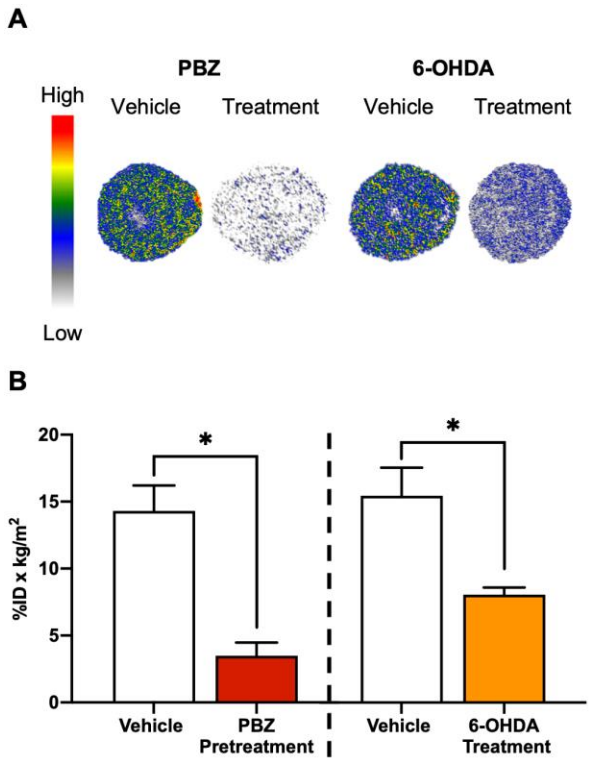

Figure 6. *Ex vivo* autoradiography of mid-ventricular short axis slices from SD rats at 30 minutes. (n = 2 animals per group). * Statistical significance reached by unpaired two-tailed t-test (p <0.05).

Clearance of myocardial [^{18}F]mFBG is independent of uptake-1 and uptake-2. Next, we were keen to determine the clearance mechanism of [^{18}F]mFBG in the myocardium and performed DMI- and PBZ-chase experiments with PET imaging (Figure 7). Each pharmacological treatment was administered after peak LV accumulation (10 minutes after tracer injection), and differences in tracer washout were quantified by k_{mono}. Animals treated with DMI chase (0.023 ± 0.004 min^{-1}), and PBZ chase (0.035 ± 0.008 min^{-1}) were not found to have significantly increased washout compared to animals administered vehicle chase treatment (0.027 ± 0.002 min^{-1}). DMI chase insensitivity suggests minimal activity reuptake by NET, consistent with the lower affinity of [^{18}F]mFBG for NET. Other benzylguanidine radiotracers have similarly shown insensitivity to DMI-chase treatment in higher species, which is attributed to irreversible intraneuronal vesicular

trapping.[53] PBZ chase insensitivity supports the notion of insignificant [^{18}F]mFBG reuptake through extraneuronal transporters. Based on our tracer stability results, the observed washout of radioactivity is unlikely to be the result of an excreted metabolite. Similarly, the high degree of myocardial washout over 60 minutes and good quality of monoexponential fits for these data suggest that selective clearance from myocytes along with neuronal retention is improbable. Importantly, human imaging studies, where uptake-2 contributes less to benzylguanidine uptake, have also revealed rapid washout uniquely for [^{18}F]mFBG.[26] Therefore, the absence of increased tracer washout from the myocardium upon inhibition of uptake-1 and uptake-2 mechanisms following peak activity accumulation suggests that [^{18}F]mFBG clearance to plasma predominates over reuptake by these transporters.

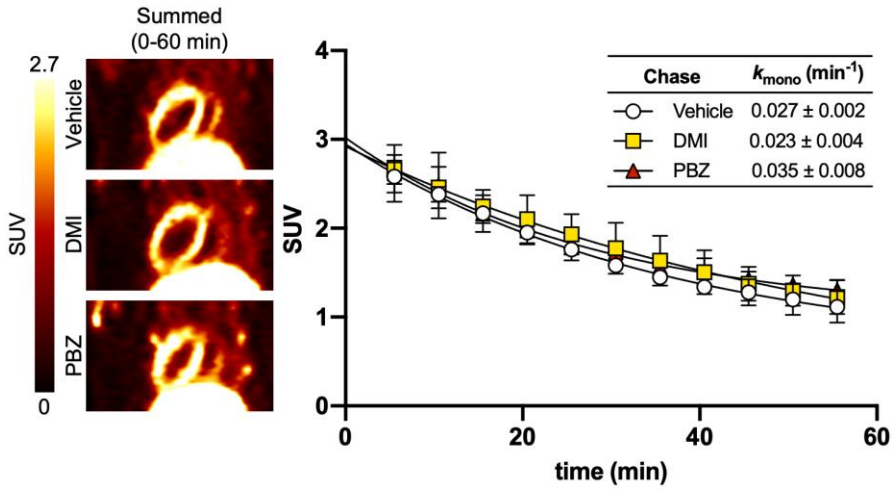

Figure 7. *In* vivo PET imaging of the myocardium in SD rats following chase dosing with vehicle, DMI, and PBZ at 10 minutes (n = 3 per group).

Conclusions

A reliable and efficient automated synthesis of [^{18}F]mFBG in high molar activity has been developed, enabling preclinical evaluation for cardiac sympathetic nerve imaging. Our *in vivo*

investigation of [^{18}F]mFBG in Sprague Dawley rats showed clear delineation of the left ventricle with tracer washout following a monoexponential fit after 5 minutes. [^{18}F]mFBG stability studies revealed >97% of the parent tracer in the myocardium with moderate parent fraction in plasma at an equivalent time-point. No significant differences between sexes were identified for baseline myocardial uptake and parent fraction in tissue or plasma. [^{18}F]mFBG, in comparison to its benzylguanidine analogues [^{123}I]mIBG and [^{18}F]FBBG, possesses unique NET dependent neuronal uptake in rats evidenced by pre-treatment blockade with DMI and 6-OHDA sympathectomy. Extraneuronal uptake-2 dependent mechanisms also contribute significantly to radiotracer accumulation. These results were further supported by PET imaging and *ex vivo* autoradiography. Chase-dosing experiments with DMI and PBZ demonstrated insignificant radiotracer recycling in the myocardium through uptake-1 and uptake-2 transporters, which is distinct from the neurotransmitter analogue [^{11}C]HED. In summary, [^{18}F]mFBG is a promising radiotracer candidate that displays favourable imaging properties and unique myocardial clearance with the potential for accurate quantification of SNS dysfunction using PET imaging in rats and higher species.

Methods

Chemistry. The synthetic procedure for the preparation of the [^{18}F]mFBG precursor (**4**), including the synthesis of SPIAd (**3**) was performed as previously described.[35]

N′,*N″*-di(*tert*-butoxy)carbonyl-*meta*-iodobenzylguanidine (**1**). A solution of 1,3-bis(*tert*-butoxycarbonyl)-2-methyl-2-thiopseudourea (1.2 mmol) in DMF (0.5 mL) was added to a flask containing *meta*-iodobenzylamine hydrochloride (1 mmol) and triethylamine (3 mmol) dissolved in DMF (0.5 mL). The reaction was stirred at room temperature overnight, diluted with ethyl acetate, and washed with water (3×), then brine (3×). The organic layers were pooled and dried

with magnesium sulfate, filtered, and concentrated under reduced pressure. The residue was purified by flash column chromatography (0–25% hexane/ethyl acetate) to yield the final product as a white solid (437 mg, 92%). ^{1}H NMR (600 MHz, $CDCl_3$): δ 11.53 (s, 1H), 8.58 (s, 1H), 7.67 (s, 1H), 7.61 (d, *J* = 7.8 Hz, 1H), 7.28 (d, *J* = 7.7 Hz, 1H), 7.08 (t, *J* =7.8 Hz, 1H), 4.57 (d, *J* = 5.4 Hz, 2H), 1.51 (s, 9H), 1.49 (s, 9H) ppm. ^{13}C NMR (151 MHz, $CDCl_3$): δ 163.5, 156.1, 153.2, 139.8, 136.9, 136.7, 130.4, 127.1, 94.5, 83.3, 79.5, 44.1, 28.3, 28.0, ppm.

N,*N*′,*N*′,*N*″-tetra(*tert*-butoxy)carbonyl-*meta*-iodobenzylguanidine (**2**). To a solution of **1** (0.92 mmol) in THF (6.12 mL) was added *N*,*N*-dimethylaminopyridine (4.6 mmol). The reaction was cooled to 0 °C and di-*tert*-butyl dicarbonate (3.45 mmol) was added over ten minutes. The reaction was then stirred at room temperature for two hours and concentrated under reduced pressure. The residue was resuspended in ethyl acetate, and the organic layer was washed with water (3×). The organic fractions were collected, dried with magnesium sulfate, filtered, concentrated under reduced pressure, and purified by flash chromatography (0–25% hexane/ethyl acetate) to yield the final product as a colorless oil (571 mg, 92%). ^{1}H NMR (400 MHz, $CDCl_3$): δ 7.71 (s, 1H), 7.55 (d, *J* = 7.9 Hz, 1H), 7.37 (d, *J* = 7.8 Hz, 1H), 7.01 (t, *J* = 7.7 Hz, 1H), 4.93 (s, 2H), 1.46 (s, 9H), 1.42 (s, 18H), 1.38 (s, 9H) ppm. ^{13}C NMR (101 MHz, $CDCl_3$): δ 157.2, 151.1, 147.2, 144.4, 139.8, 136.8, 136.3, 130.0, 127.2, 94.0, 84.0, 83.7, 82.0, 49.3, 28.0, 27.9, 27.8 ppm.

spiroadamantyl-1,3-dioxane-4,6-dione (**3**). Malonic acid (4.8 mmol), acetic anhydride (5.1 mmol, 0.5 mL), and H_2SO_4 (1 drop) were stirred at 60 °C for 15 minutes, then cooled to room temperature. 2-Adamantanone (4.8 mmol) was added dropwise over 0.5–1 hr, and the mixture was stirred at room temperature for an additional 1 hr. The reaction was concentrated under reduced pressure, reconstituted in dichloromethane (DCM) then washed with water (3×), dried with magnesium sulfate, and filtered. The crude was concentrated under reduced pressure and

recrystallized using hexane and ethyl acetate to yield the final product as white crystals (680 mg, 60%).[1]H NMR (600 MHz, $CDCl_3$) δ 3.60 (s, 2H), 2.18–2.10 (m, 6H), 1.89 (s, 2H), 1.79–1.73 (m, 6H). [13]C NMR (151 MHz, $CDCl_3$) δ 163.1, 109.6, 37.6, 36.7, 36.5, 33.5, 26.1 ppm.

N,*N*′,*N*′,*N*″-tetra(*tert*-butoxy)carbonyl-*meta*-(spiroadamantyl-1,3-dioxane-4,6-dione-5-ylidene)iodobenzylguanidine (**4**). Compound **2** (1.1 mmol) was dissolved in anhydrous acetonitrile (ACN, 6.8 mL) and TMSOAc (2.86 mmol) was added. Then, a slurry of Selectfluor (1.43 mmol) in ACN (6.8 mL) was added to the reaction and left to stir overnight. The crude mixture was then concentrated under pressure and resuspended in DCM (10 mL). The solution was filtered by gravity filtration, and the filtrate was collected, concentrated, and resuspended in EtOH (4.4 mL). A solution of **3** (1.1 mmol) dissolved in a 10% aqueous bicarbonate solution (3.7 mL) was then added dropwise to the reaction. After 6 hours, the contents of the flask were concentrated under reduced pressure and purified by column chromatography (0–100% hexane/ethyl acetate) to yield the final product as an off-white powder (415 mg, 41%). [1]H NMR (600 MHz, $CDCl_3$): δ 7.86 (s, 1H), 7.73 (d, *J* = 8.4 Hz, 1H), 7.64 (d, *J* = 7.8 Hz, 1H), 7.34 (t, *J* = 7.9 Hz, 1H), 5.00 (s, 2H), 2.41 (s, 2H), 2.16 (s, 2H), 2.14 (s, 2H), 1.84 (s, 2H), 1.69 (s, 4H), 1.67 (s, 2H), 1.48 (s, 9H), 1.45 (s, 18H), 1.40 (s, 9H) ppm. [13]C NMR (151 MHz, CDCl3): δ 163.4, 157.2, 150.9, 147.3, 144.5, 142.0, 132.4, 131.9, 131.7, 114.0, 107.5, 84.7, 84.1, 84.0, 82.4, 55.5, 49.5, 37.2, 35.6, 33.7, 33.5, 28.8, 28.0, 26.5 ppm.

meta-fluorobenzylguanidine hydrochloride (**6**). The non-radioactive standard (mFBG, **6**) was synthesized following the guanylation procedure outlined for the synthesis of compound **1** using *meta*-fluorobenzylamine (0.12 mmol). The partially Boc-protected intermediate (0.18 mmol, **5a**) was concentrated, and resuspended in dioxane, followed by the addition of excess 4.0 M HCl in dioxane. The reaction was left to stir for 15 min, and the residue was concentrated under reduced

pressure. The product was precipitated (5×) using methanol and *tert*-butyl methyl ether to yield the final product as a white powder (27 mg, 88%). ^{1}H NMR (600 MHz, DMSO): δ = 8.25 (br, 1H), 7.90-6.90 (br, 3H), 7.46-7.40 (m, 1H), 7.18-7.12 (m, 3H), 4.42 (d, J = 6.0 Hz, 2H). ^{13}C NMR (151 MHz, DMSO): δ = 163.5 (d, J = 244.0 Hz), 157.6, 140.9 (d, J = 7.0 Hz), 131.1 (d, J = 8.3 Hz), 123.7 (d, J = 2.8 Hz), 114.8 (d, J = 21.0.8 Hz), 114.5 (d, J = 22.1 Hz), 43.8.^{19}F NMR (377 MHz, DMSO): δ = -113.1 (s, 1F). The product was characterized in accordance with the literature.[31]

Radiochemistry. Aqueous [^{18}F]fluoride (no-carrier-added) was produced by a Siemens CTI Eclipse HP/RD Hybrid Cyclotron (11 MeV) via an ^{18}O(p,n)^{18}F nuclear reaction and delivered to a hot cell. A solution of TEAB (4 mg in 1 mL of MeCN) was added to an aliquot of target water (≤ 1 mL) containing a suitable amount of [^{18}F]fluoride in a sealed conical vial equipped with a vent needle. The vial was placed in a heating block and dried under nitrogen flow (passed over a P_2O_5-Drieriete™ column) at 100 °C. Acetonitrile (1 mL) was added to the dried residue, and heating was resumed until the liquid was completely evaporated. This process was repeated three times. Subsequently, the contents of the vial were resolubilized in the desired solvent (0.3 mL) containing precursor **4** (6 mg) and then heated at the desired temperature for 5, 10, 15, or 20 min. An aliquot of the crude reaction was spotted onto a silica plate developed in a chamber containing ethyl acetate, and crude yields were determined by radioTLC. Aqueous HCl (0.2 mL, 6 or 12 M) was then added to the vial and heated at the desired temperature (100 °C or 120 °C) for 5, 10, 15, or 20 min. Following completion, the reaction was partially neutralized with NaOH (0.2 mL, 8 M) and the mixture was sampled for radioTLC analysis. An additional sample was prepared to verify the yield by radioHPLC using a Waters 2695 Alliance HPLC equipped with a Phenomenex Luna 10 µm C18(2) (100 Å, 250 mm × 4.6 mm) column, a 996 Photodiode Array Detector (Waters), and a Carroll & Ramsey Associates 105-S high-sensitivity radiation detector. Gradient: 1/99 10 mM

PBS/ACN for 1 min, linear gradient to 80/20 over 8 min, isocratic for 7 minutes, then linear gradient back to 1/99 over 3 minutes. Retention time: ~15 min, flow rate = 1 mL/min.

Automated radiosynthesis. A fully automated sequence was developed on a GE TRACERlab™ FX2N module to prepare [^{18}F]mFBG. The reagents were loaded as follows: TEAB (4 mg in 0.8 mL H_2O) in vial 1; HCl (0.6 mL, 12 M) in vial 2; precursor **4** (12 mg in 0.6 mL DMSO) in vial 3; ACN (1 mL) in vial 4; H_2O (0.6 mL) in vial 5; ACN/H_2O (30/70, 1.3 mL) in vial 6. A Sep-pak Carboxy Methyl (CM) ion exchange cartridge (preconditioned with 10 mL of EtOH and 10 mL of H_2O) was also installed. [^{18}F]Fluoride (~11 GBq) was captured from the [^{18}O]H_2O target solution using a Sep-pak Accel Plus QMA Plus Light cartridge (preconditioned using 10 mL of EtOH, 10 mL of H_2O, 10 mL of 0.1 M $NaHCO_3$, and 10 mL H_2O), and eluted into the reactor by unloading vial 1. After unloading vial 4, the reactor was heated to 80 °C for 5 minutes, and 120 °C for 3 minutes under a nitrogen stream to yield dried [^{18}F]TEAF. The reactor was then cooled to 40 °C using compressed air, before initiating the reaction by unloading vial 3. The radiofluorination reaction was performed at 120 °C for 10 minutes and subsequently cooled to 50 °C. Acidic deprotection was initiated by unloading vial 2 and heating the reactor to 120 °C for 5 minutes. Following cooling with compressed air, the reaction was quenched with the contents of vial 5 and transferred to an adjacent vial. The reactor was further rinsed with the contents of vial 6 and collected in the same vial. The crude mixture was purified by reversed phase HPLC (Phenomenex Luna 10 µm C18(2), 250 x 10 mm, isocratic 30/70 ACN/H_2O + 0.1% TFA, flow rate of 5 mL/min). The product was collected from 13–15 min into a bulk vessel containing 20 mL of sterile water. The contents of this vessel were passed through the CM cartridge at a flow rate of 2.5 mL/min and rinsed with H_2O (10 mL). [^{18}F]mFBG was eluted with physiological saline (4 mL) and passed through a sterile filter into a crimped vial fitted with a vent needle. Radiochemical yield

(RCY) was determined by decay correcting the amount of initial activity to the end of synthesis (EoS). Molar activity was determined by measurement of the UV absorbance of a known amount of radioactivity under identical HPLC conditions used to generate a calibration curve for the corresponding non-radioactive standard. The ratio of radioactivity (GBq) to moles (μmol) provided the molar activity (GBq/μmol), which was decay corrected to the end of synthesis (EoS).

Animal care. Male and female Sprague-Dawley rats (80–110 g) were purchased from Charles River Laboratories (Senneville, Quebec) and housed in environmentally enriched cages with free access to food and water. All housing, handling, and experimental procedures were in strict accordance with the guidelines of Canadian Council on Animal Care and with approval of the University of Ottawa Animal Care Committee. Animals used in this study were 4 weeks old unless specified otherwise.

PET imaging. Male and female Sprague-Dawley rats (4–8 weeks old, 80–270 g) were anesthetized with 2% isoflurane and placed in the PET scanner. Following a 10-minute transmission scan, the animals were injected with [^{18}F]mFBG as a bolus over 30 seconds via the lateral tail vein and maintained under isoflurane during the imaging protocol. Whole body PET imaging was performed for 60 minutes (4 × 15 sec frames; 4 × 1 min frames; 10 × 5 min frames) using a Siemens DPET scanner. The collected emission data was corrected for attenuation and scatter and reconstructed using the 3D-OSEM/MAP algorithm. Volumes of interest (VOI) were drawn for the left ventricle and cardiac blood pool using FlowQuant™. Blood pool time-activity curves were created from mean values of three samples located in the left ventricle cavity, the left ventricle base, and the left atrium. Polar maps were also generated by FlowQuant™. Uptake values were obtained in nCi/cc and converted to SUV using the total injected dose and animal bodyweight, as shown in the time-activity curves.

***Ex vivo* pharmacological blocking studies.** Male and female Sprague Dawley rats were anesthetized using 2% isoflurane and received lateral tail-vein injections of 4–13 MBq of [^{18}F]mFBG in 0.15–0.3 mL of sterile saline (0.9% sodium chloride). For animals requiring pharmacological treatment, DMI (1 mg/kg), PBZ (27 ± 3 mg/kg), or saline was administered via the lateral tail vein 10 minutes prior to radiotracer injection. Baseline studies were conducted without pretreatment. Subsequently, anesthesia was stopped, and the animals were allowed to recover. After thirty minutes, the animals were sacrificed by CO_2 asphyxiation followed by cervical dislocation. All organs were harvested (blood collected by cardiac puncture), weighed, and counted for radioactivity in a gamma counter (Hidex Automatic Gamma Counter, Energy window: 480–558 keV). Counts per minute (CPM) were converted to activity using a set of calibration standards with known activities. Percentage injected dose (%ID) was calculated from dividing the organ activity by the injected dose (decay-corrected) and further normalized by sample mass to obtain the percentage injected dose per gram tissue (%ID/g).

Note: Due to the poor solubility of PBZ in physiological saline, a 20 mg/mL suspension of PBZ was prepared and filtered through a 0.45 µm filter. A known volume of the effluent was sampled on a Waters Xevo TQD with an Acquity UPLC H-Class Plus system, and the concentration of the solution was determined using a calibration curve (Figure S11).

6-OHDA treatment. Male Sprague Dawley rats (80–110 g) were acclimatized for one week upon arrival, then given the previously reported treatment cycle (Figure S7).[46] Briefly, animals were treated with either vehicle (saline + 0.1% ascorbate) or 6-OHDA via the lateral tail vein as a bolus injection. Animals were dosed twice on day 1 (morning and afternoon, 50 mg/kg), and twice on day 7 (morning and afternoon, 100 mg/kg). On day 14, the animals were administered [^{18}F]mFBG,

and organs were harvested, counted for radioactivity, and weighed. Alternatively, vehicle and 6-OHDA treated rats were subject to PET imaging, as previously described.

Parent Fraction in Plasma and Myocardium. Male and female Sprague Dawley rats (80–110 g) were injected with [^{18}F]mFBG. Blood samples (500–1200 µL) were obtained via cardiac puncture at the 30-minute time-point and placed in a heparinized tube. Samples were centrifuged at 4 °C for 7 minutes at 4000 rpm, and the plasma fraction was isolated. Protein free plasma (PFP) was obtained by the addition of an equal volume of ice-cold ACN, followed by centrifugation at 4 °C for 5 minutes at 4000 rpm. The myocardium was perfused with 15 mL of 1× PBS, cut into small pieces, and placed into separate tubes containing a 50/50 mixture of ACN/H_2O. The tubes were placed in an ice bath and homogenized using a Fisher Scientific PowerGen 125 (125 W, 115 V, 50/60 Hz) adapted with a sawtooth, 7 × 95 mm generator. Samples were then centrifuged at 4 °C for 5 minutes at 4000 rpm. For both plasma and myocardium preparations, additional extractions were performed until extraction efficiency was ≥70%, as measured on a gamma counter. The supernatants were then filtered through a 0.22 µm filter, spiked with non-radioactive standard (10 µL, 1 mg/mL), and injected onto the analytical radioHPLC. Fractions were collected every minute, for 20 minutes, and placed on the gamma counter to determine the total activity in each fraction.

Autoradiography. Sprague Dawley rats were administered vehicle or pharmacological treatment prior to receiving [^{18}F]mFBG, as described above. After 30 minutes, hearts were perfused with 15 mL of 1× PBS and harvested. Samples were embedded with OCT, flash frozen, sliced into 10 µm sections using a Thermofisher Science Microm HM 550 cryostat. Tissue sections from the apex to the base were obtained by slicing along the short axis of the heart. The sections were immediately exposed to a super-resolution Storage Phosphor Screen (BAS-IP SR 2025 E) in an Electrophoresis Systems Autoradiography Cassette (FBXC 810) overnight. The images were obtained using a

Cyclone Plus Storage Phosphor System and images were analyzed using OptiQuant. ROIs were drawn for the whole myocardium and digital light units (DLU) were converted to activity using a using a set of calibration standards with known activities on the same screen. Percentage injected dose (%ID) was calculated by dividing the ROI activity by the injected dose (decay-corrected) and further normalized by area (m^2) and animal weight (kg) to obtain weight-normalized activity density (%ID×kg/m^2).

Statistical Analysis. Statistical analysis was performed using GraphPad Prism. Significance was set at the 0.05 level. The data are presented as mean ± standard deviation. Differences between two groups were tested using a 2-tailed unpaired Student's t-test.

Associated Content

Supporting Information. General experimental information; synthetic procedures and characterization; precursor stability; radiofluorination regioselectivity; experimental timeline; whole body and regional myocardial imaging analysis. This material is available free of charge via the Internet at http://pubs.acs.org

Author information

Corresponding author* Molecular Imaging Probes and Radiochemistry Research Laboratory. University of Ottawa Heart Institute Ottawa K1Y 4W7, Canada. Department of Biochemistry, Microbiology and Immunology and Department of Chemistry and Biomolecular Sciences, University of Ottawa. E-mail: benjamin.rotstein@uottawa.ca

Acknowledgements

We thank the staff of the University of Ottawa Heart Institute PET Radiochemistry Laboratory and Biomedical Engineering for cyclotron and small animal PET scanner support. Financial support from the Heart & Stroke Foundation of Canada and CANet (PG-17-0736 to B.H.R.), CFI (JELF 36848 to B.H.R.), the Province of Ontario (ER17-13-119 to B.H.R.) and the University of Ottawa Heart Institute are gratefully acknowledged. Scholarship support was received from the Province of Ontario (A.B. & G.F.), CIHR (G.F.), and the IIE Fulbright Program (A.P.).

Abbreviations

[^{18}F]3F-PHPG, 3-[^{18}F]fluoro-*para*-hydroxyphenethylguanidine; [^{18}F]4F-MHPG, 4-[^{18}F]fluoro-*meta*-hydroxyphenethylguanidine; 6-OHDA, 6-hydroxydopamine; CM, carboxymethyl; DMI, desipramine; EoS, end of synthesis; [^{18}F]FBBG, [^{18}F]flubrobenguane; HLB, hydrophilic lipophilic balance; LV, left ventricle; [^{18}F]mFPBG, *meta*-(3-[^{18}F]fluoropropyl)benzylguanidine; [^{18}F]mFBG, *meta*-[^{18}F]fluorobenzylguanidine; [^{123}I]mIBG, *meta*-[^{123}I]iodobenzylguanidine; [^{11}C]HED, *meta*-[^{11}C]hydroxyephedrine; NET, norepinephrine transporter; PBZ, phenoxybenzamine; PET, positron emission tomography; QMA, quaternary methyl ammonium; RCY, radiochemical yield; RE, reformulation efficiency; SUV, standardized uptake value; SNS, sympathetic nervous system; VMAT, vesicular monoamine transporter;

References

(1) Jamali, H. K.; Waqar, F.; Gerson, M. C. Cardiac Autonomic Innervation. *J. Nucl. Cardiol.* **2017**, *24* (5), 1558–1570. https://doi.org/10.1007/s12350-016-0725-7.

(2) Zelt, J. G. E.; deKemp, R. A.; Rotstein, B. H.; Nair, G. M.; Narula, J.; Ahmadi, A.; Beanlands, R. S.; Mielniczuk, L. M. Nuclear Imaging of the Cardiac Sympathetic Nervous System: A Disease-Specific Interpretation in Heart Failure. *JACC Cardiovasc. Imaging* **2020**, *13* (4), 1036–1054. https://doi.org/10.1016/j.jcmg.2019.01.042.

(3) van der Bijl, P.; Knuuti, J.; Delgado, V.; Bax, J. J. Cardiac Sympathetic Innervation Imaging with PET Radiotracers. *Curr. Cardiol. Rep.* **2021**, *23* (1), 4. https://doi.org/10.1007/s11886-020-01432-9.

(4) Franciosi, S.; Perry, F. K. G.; Roston, T. M.; Armstrong, K. R.; Claydon, V. E.; Sanatani, S. The Role of the Autonomic Nervous System in Arrhythmias and Sudden Cardiac Death. *Auton. Neurosci.* **2017**, *205*, 1–11. https://doi.org/10.1016/j.autneu.2017.03.005.

(5) Jungen, C.; Scherschel, K.; Flenner, F.; Jee, H.; Rajendran, P.; De Jong, K. A.; Nikolaev, V.; Meyer, C.; Ardell, J. L.; Tompkins, J. D. Increased Arrhythmia Susceptibility in Type 2 Diabetic Mice Related to Dysregulation of Ventricular Sympathetic Innervation. *Am. J. Physiol.-Heart Circ. Physiol.* **2019**, *317* (6), H1328–H1341. https://doi.org/10.1152/ajpheart.00249.2019.

(6) Fisher, V. L.; Tahrani, A. A. Cardiac Autonomic Neuropathy in Patients with Diabetes Mellitus: Current Perspectives. *Diabetes Metab. Syndr. Obes. Targets Ther.* **2017**, *10*, 419–434. https://doi.org/10.2147/DMSO.S129797.

(7) Farber, G.; Boczar, K. E.; Wiefels, C. C.; Zelt, J. G. E.; Guler, E. C.; deKemp, R. A.; Beanlands, R. S.; Rotstein, B. H. The Future of Cardiac Molecular Imaging. *Semin. Nucl. Med.* **2020**, *50* (4), 367–385. https://doi.org/10.1053/j.semnuclmed.2020.02.005.

(8) Boutagy, N. E.; Sinusas, A. J. Recent Advances and Clinical Applications of PET Cardiac Autonomic Nervous System Imaging. *Curr. Cardiol. Rep.* **2017**, *19* (4), 33. https://doi.org/10.1007/s11886-017-0843-0.

(9) Thackeray, J. T.; Bengel, F. M. Assessment of Cardiac Autonomic Neuronal Function Using PET Imaging. *J. Nucl. Cardiol.* **2013**, *20* (1), 150–165. https://doi.org/10.1007/s12350-012-9644-4.

(10) Jacobson, A. F.; Senior, R.; Cerqueira, M. D.; Wong, N. D.; Thomas, G. S.; Lopez, V. A.; Agostini, D.; Weiland, F.; Chandna, H.; Narula, J.; ADMIRE-HF Investigators. Myocardial Iodine-123 Meta-Iodobenzylguanidine Imaging and Cardiac Events in Heart Failure. Results of the Prospective ADMIRE-HF (AdreView Myocardial Imaging for Risk Evaluation in Heart Failure) Study. *J. Am. Coll. Cardiol.* **2010**, *55* (20), 2212–2221. https://doi.org/10.1016/j.jacc.2010.01.014.

(11) Fallavollita, J. A.; Heavey, B. M.; Luisi, A. J.; Michalek, S. M.; Baldwa, S.; Mashtare, T. L.; Hutson, A. D.; Dekemp, R. A.; Haka, M. S.; Sajjad, M.; Cimato, T. R.; Curtis, A. B.; Cain, M. E.; Canty, J. M. Regional Myocardial Sympathetic Denervation Predicts the Risk of Sudden Cardiac Arrest in Ischemic Cardiomyopathy. *J. Am. Coll. Cardiol.* **2014**, *63* (2), 141–149. https://doi.org/10.1016/j.jacc.2013.07.096.

(12) Chen, X.; Kudo, T.; Lapa, C.; Buck, A.; Higuchi, T. Recent Advances in Radiotracers Targeting Norepinephrine Transporter: Structural Development and Radiolabeling Improvements. *J. Neural Transm.* **2020**, *127* (6), 851–873. https://doi.org/10.1007/s00702-020-02180-4.

(13) Langer, O.; Halldin, C. PET and SPET Tracers for Mapping the Cardiac Nervous System. *Eur. J. Nucl. Med. Mol. Imaging* **2002**, *29* (3), 416–434. https://doi.org/10.1007/s002590100640.

(14) Travin, M. I. Imaging of Cardiac Autonomic Innervation with SPECT and PET. *Curr. Cardiovasc. Imaging Rep.* **2013**, *7* (1), 9242. https://doi.org/10.1007/s12410-013-9242-0.

(15) Raffel, D. M.; Jung, Y.-W.; Gildersleeve, D. L.; Sherman, P. S.; Moskwa, J. J.; Tluczek, L. J.; Chen, W. Radiolabeled Phenethylguanidines: Novel Imaging Agents for Cardiac Sympathetic Neurons and Adrenergic Tumors. *J. Med. Chem.* **2007**, *50* (9), 2078–2088. https://doi.org/10.1021/jm061398y.

(16) Jang, K. S.; Jung, Y.-W.; Gu, G.; Koeppe, R. A.; Sherman, P. S.; Quesada, C. A.; Raffel, D. M. 4-[^{18}F]Fluoro-m-Hydroxyphenethylguanidine: A Radiopharmaceutical for Quantifying Regional Cardiac Sympathetic Nerve Density with Positron Emission Tomography. *J. Med. Chem.* **2013**, *56* (18), 7312–7323. https://doi.org/10.1021/jm400770g.

(17) Raffel, D. M.; Wieland, D. M. Assessment of Cardiac Sympathetic Nerve Integrity with Positron Emission Tomography. *Nucl. Med. Biol.* **2001**, *28* (5), 541–559. https://doi.org/10.1016/s0969-8051(01)00210-4.

(18) Bengel, F. M.; Schwaiger, M. Assessment of Cardiac Sympathetic Neuronal Function Using PET Imaging. *J. Nucl. Cardiol.* **2004**, *11* (5), 603–616. https://doi.org/10.1016/j.nuclcard.2004.06.133.

(19) Woo, S.-K.; Moon, B. S.; Kim, B. S.; Kim, M. H.; Lee, Y. J.; Jung, J. H.; Lee, K. C.; Seo, Y.; Kim, W.; Lim, S. M.; Lee, B. C.; Kim, S. E. Feasibility of Myocardial PET Imaging Using a Benzylguanidine Analog: Meta-(3-[^{18}F]Fluoropropyl)Benzylguanidine

([^{18}F]MFPBG). *Nucl. Med. Biol.* **2018**, *61*, 63–70. https://doi.org/10.1016/j.nucmedbio.2018.04.005.

(20) Raffel, D. M.; Jung, Y.-W.; Koeppe, R. A.; Jang, K S.; Gu, G.; Scott, P. J.H.; Murthy, V. L.; Rothley, J.; Frey, K. A. First-in-Human Studies of [^{18}F] Fluorohydroxyphenethylguanidines. *Circ. Cardiovasc. Imaging* **2018**, *11* (12), e007965. https://doi.org/10.1161/CIRCIMAGING.118.007965.

(21) Jung, Y.-W.; Jang, K. S.; Gu, G.; Koeppe, R. A.; Sherman, P. S.; Quesada, C. A.; Raffel, D. M. [^{18}F]Fluoro-Hydroxyphenethylguanidines: Efficient Synthesis and Comparison of Two Structural Isomers as Radiotracers of Cardiac Sympathetic Innervation. *ACS Chem. Neurosci.* **2017**, *8* (7), 1530–1542. https://doi.org/10.1021/acschemneuro.7b00051.

(22) Jung, Y.-W.; Gu, G.; Raffel, D. M. Improved Synthesis of 4-[^{18}F]Fluoro-m-Hydroxyphenethylguanidine Using an Iodonium Ylide Precursor. *J. Label. Compd. Radiopharm.* **2019**, *62* (12), 835–842. https://doi.org/10.1002/jlcr.3791.

(23) Chen, X.; Fritz, A.; Werner, R. A.; Nose, N.; Yagi, Y.; Kimura, H.; Rowe, S. P.; Koshino, K.; Decker, M.; Higuchi, T. Initial Evaluation of AF78: A Rationally Designed Fluorine-18-Labelled PET Radiotracer Targeting Norepinephrine Transporter. *Mol Imaging Biol* **2020**, *22* (3), 602–611. https://doi.org/10.1007/s11307-019-01407-5.

(24) Garg, P.K.; Garg, S.; Zalutsky, M.R. Synthesis and Preliminary Evaluation of *para*- and *meta*-[^{18}F]Fluorobenzylguanidine. *Nucl. Med. Biol.* **1994**, *21* (1), 97–103. https://doi.org/10.1016/0969-8051(94)90135-X.

(25) Zhang, H.; Huang, R.; Pillarsetty, N.; Thorek, D. L. J.; Vaidyanathan, G.; Serganova, I.; Blasberg, R. G.; Lewis, J. S. Synthesis and Evaluation of ^{18}F-Labeled Benzylguanidine

Analogs for Targeting the Human Norepinephrine Transporter. *Eur. J. Nucl. Med. Mol. Imaging* **2014**, *41* (2), 322–332. https://doi.org/10.1007/s00259-013-2558-9.

(26) Pandit-Taskar, N.; Zanzonico, P. B.; Staton, K. D.; Carrasquillo, J. A.; Reidy-Lagunes, D.; Lyashchenko, S. K.; Burnazi, E.; Zhang, H.; Lewis, J. S.; Blasberg, R.; Larson, S. M.; Weber, W. A.; Modak, S. Biodistribution and Dosimetry of ^{18}F-Meta Fluorobenzyl Guanidine (MFBG): A First-in-Human PET-CT Imaging Study of Patients with Neuroendocrine Malignancies. *J. Nucl. Med.* **2017**. https://doi.org/10.2967/jnumed.117.193169.

(27) Glowniak, J. V.; Turner, F. E.; Gray, L. L.; Palac, R. T.; Lagunas-Solar, M. C.; Woodward, W. R. Iodine-123 Metaiodobenzylguanidine Imaging of the Heart in Idiopathic Congestive Cardiomyopathy and Cardiac Transplants. *J. Nucl. Med.* **1989**, *30* (7), 1182–1191.

(28) Takatsu, H.; Noda, T.; Arai, M.; Kunishima, A.; Inoue, M.; Tazawa, S.; Kurosawa, H.; Nishigaki, K.; Fujiwara, H. Washout of I-123 Meta-Iodobenzylguanidine for Assessing Cardiac Sympathetic Activity with Progression of Hypertension in Dahl Salt-Sensitive Rats. *J. Nucl. Cardiol.* **1999**, *6* (2), 204–210. https://doi.org/10.1016/S1071-3581(99)90081-8.

(29) Zelt, J. G. E.; Britt, D.; Mair, B. A.; Rotstein, B. H.; Quigley, S.; Walter, O.; Garrard, L.; Robinson, S.; Mielniczuk, L. M.; deKemp, R. A.; Beanlands, R. S. Regional Distribution of Fluorine-18-Flubrobenguane and Carbon-11-Hydroxyephedrine for Cardiac PET Imaging of Sympathetic Innervation. *JACC Cardiovasc. Imaging* **2020**. https://doi.org/10.1016/j.jcmg.2020.09.026.

(30) Pauwels, E.; Celen, S.; Vandamme, M.; Leysen, W.; Baete, K.; Bechter, O.; Bex, M.; Serdons, K.; Van Laere, K.; Bormans, G.; Deroose, C. M. Improved Resolution and Sensitivity of [^{18}F]MFBG PET Compared with [^{123}I]MIBG SPECT in a Patient with a

Norepinephrine Transporter–Expressing Tumour. *Eur. J. Nucl. Med. Mol. Imaging* **2021**, *48* (1), 313–315. https://doi.org/10.1007/s00259-020-04830-x.

(31) Preshlock, S.; Calderwood, S.; Verhoog, S.; Tredwell, M.; Huiban, M.; Hienzsch, A.; Gruber, S.; Wilson, T. C.; Taylor, N. J.; Cailly, T.; Schedler, M.; Collier, T. L.; Passchier, J.; Smits, R.; Mollitor, J.; Hoepping, A.; Mueller, M.; Genicot, C.; Mercier, J.; Gouverneur, V. Enhanced Copper-Mediated ^{18}F-Fluorination of Aryl Boronic Esters Provides Eight Radiotracers for PET Applications. *Chem. Commun.* **2016**, *52* (54), 8361–8364. https://doi.org/10.1039/C6CC03295H.

(32) Turnock, S.; Turton, D. R.; Martins, C. D.; Chesler, L.; Wilson, T. C.; Gouverneur, V.; Smith, G.; Kramer-Marek, G. ^{18}F-Meta-Fluorobenzylguanidine (^{18}F-mFBG) to Monitor Changes in Norepinephrine Transporter Expression in Response to Therapeutic Intervention in Neuroblastoma Models. *Sci. Rep.* **2020**, *10* (1), 20918. https://doi.org/10.1038/s41598-020-77788-3.

(33) Zhang, H.; Huang, R.; Cheung, N.-K. V.; Guo, H.; Zanzonico, P. B.; Thaler, H. T.; Lewis, J. S.; Blasberg, R. G. Imaging the Norepinephrine Transporter in Neuroblastoma: A Comparison of [^{18}F]-MFBG and ^{123}I-MIBG. *Clin. Cancer Res.* **2014**, *20* (8), 2182–2191. https://doi.org/10.1158/1078-0432.CCR-13-1153.

(34) Hu, B.; Vāvere, A. L.; Neumann, K. D.; Shulkin, B. L.; DiMagno, S. G.; Snyder, S. E. A Practical, Automated Synthesis of *meta*-[^{18}F]Fluorobenzylguanidine for Clinical Use. *ACS Chem. Neurosci.* **2015**, *6* (11), 1870–1879. https://doi.org/10.1021/acschemneuro.5b00202.

(35) Rotstein, B. H.; Wang, L.; Liu, R. Y.; Patteson, J.; Kwan, E. E.; Vasdev, N.; Liang, S. H. Mechanistic Studies and Radiofluorination of Structurally Diverse Pharmaceuticals with

Spirocyclic Iodonium(III) Ylides. *Chem. Sci.* **2016**, *7* (7), 4407–4417. https://doi.org/10.1039/C6SC00197A.

(36) Qin, L.; Hu, B.; Neumann, K. D.; Linstad, E. J.; McCauley, K.; Veness, J.; Kempinger, J. J.; DiMagno, S. G. A Mild and General One-Pot Synthesis of Densely Functionalized Diaryliodonium Salts. *Eur. J. Org. Chem.* **2015**, *2015* (27), 5919–5924. https://doi.org/10.1002/ejoc.201500986.

(37) Rotstein, B. H.; Stephenson, N. A.; Vasdev, N.; Liang, S. H. Spirocyclic Hypervalent Iodine(III)-Mediated Radiofluorination of Non-Activated and Hindered Aromatics. *Nat. Commun.* **2014**, *5* (1), 4365. https://doi.org/10.1038/ncomms5365.

(38) Cardinale, J.; Ermert, J.; Humpert, S.; Coenen, H. H. Iodonium Ylides for One-Step, No-Carrier-Added Radiofluorination of Electron Rich Arenes, Exemplified with 4-(([^{18}F]Fluorophenoxy)-Phenylmethyl)Piperidine NET and SERT Ligands. *RSC Adv.* **2014**, *4* (33), 17293–17299. https://doi.org/10.1039/C4RA00674G.

(39) Yu, M.; Bozek, J.; Lamoy, M.; Guaraldi, M.; Silva, P.; Kagan, M.; Yalamanchili, P.; Onthank, D.; Mistry, M.; Lazewatsky, J.; Broekema, M.; Radeke, H.; Purohit, A.; Cdebaca, M.; Azure, M.; Cesati, R.; Casebier, D.; Robinson, S. P. Evaluation of LMI1195, a Novel ^{18}F-Labeled Cardiac Neuronal PET Imaging Agent, in Cells and Animal Models. *Circulation: Cardiovascular Imaging* **2011**, *4* (4), 435–443. https://doi.org/10.1161/CIRCIMAGING.110.962126.

(40) Vaidyanathan, G.; McDougald, D.; Koumarianou, E.; Choi, J.; Hens, M.; Zalutsky, M. R. Synthesis and Evaluation of 4-[^{18}F]Fluoropropoxy-3-Iodobenzylguanidine ([^{18}F]FPOIBG): A Novel 18F-Labeled Analogue of MIBG. *Nucl. Med. Biol.* **2015**, *42* (8), 673–684. https://doi.org/10.1016/j.nucmedbio.2015.04.005.

(41) Sinusas, A. J.; Lazewatsky, J.; Brunetti, J.; Heller, G.; Srivastava, A.; Liu, Y.-H.; Sparks, R.; Puretskiy, A.; Lin, S.; Crane, P.; Carson, R. E.; Lee, L. V. Biodistribution and Radiation Dosimetry of LMI1195: First-in-Human Study of a Novel ^{18}F-Labeled Tracer for Imaging Myocardial Innervation. *J. Nucl. Med.* **2014**, *55* (9), 1445–1451. https://doi.org/10.2967/jnumed.114.140137.

(42) Gebhard, C. Imaging of Cardiac Sympathetic Activity in Heart Failure: Not out of the Woods Yet. *J. Nucl. Cardiol.* **2018**, *25* (4), 1172–1177. https://doi.org/10.1007/s12350-017-0779-1.

(43) Zhou, Z.; Zhen, J.; Karpowich, N. K.; Goetz, R. M.; Law, C. J.; Reith, M. E. A.; Wang, D.-N. LeuT-Desipramine Structure Reveals How Antidepressants Block Neurotransmitter Reuptake. *Science* **2007**, *317* (5843), 1390–1393. https://doi.org/10.1126/science.1147614.

(44) Ordway, G. A.; Jia, W.; Li, J.; Zhu, M.-Y.; Mandela, P.; Pan, J. Norepinephrine Transporter Function and Desipramine: Residual Drug Effects versus Short-Term Regulation. *J. Neurosci. Methods* **2005**, *143* (2), 217–225. https://doi.org/10.1016/j.jneumeth.2004.11.006.

(45) Kreusser, M. M.; Lehmann, L. H.; Haass, M.; Buss, S. J.; Katus, H. A.; Lossnitzer, D. Depletion of Cardiac Catecholamine Stores Impairs Cardiac Norepinephrine Re-Uptake by Downregulation of the Norepinephrine Transporter. *PLOS ONE* **2017**, *12* (3), e0172070. https://doi.org/10.1371/journal.pone.0172070.

(46) Thoenen, H.; Tranzer, J. P. Chemical Sympathectomy by Selective Destruction of Adrenergic Nerve Endings with 6-Hydroxydopamine. *Naunyn-Schmiedebergs Arch. Für Pharmakol. Exp. Pathol.* **1968**, *261* (3), 271–288. https://doi.org/10.1007/BF00536990.

(47) Kostrzewa, R. M.; Jacobowitz, D. M. Pharmacological Actions of 6-Hydroxydopamine. *Pharmacol. Rev.* **1974**, *26* (3), 199–288.

(48) Sachs, C.; Jonsson, G. Mechanisms of Action of 6-Hydroxydopamine. *Biochem. Pharmacol.* **1975**, *24* (1), 1–8. https://doi.org/10.1016/0006-2952(75)90304-4.

(49) Werner, R. A.; Chen, X.; Maya, Y.; Eissler, C.; Hirano, M.; Nose, N.; Wakabayashi, H.; Lapa, C.; Javadi, M. S.; Higuchi, T. The Impact of Ageing on ^{11}C-Hydroxyephedrine Uptake in the Rat Heart. *Sci. Rep.* **2018**, *8* (1), 11120. https://doi.org/10.1038/s41598-018-29509-0.

(50) Rischpler, C.; Fukushima, K.; Isoda, T.; Javadi, M. S.; Dannals, R. F.; Abraham, R.; Wahl, R.; Bengel, F. M.; Higuchi, T. Discrepant Uptake of the Radiolabeled Norepinephrine Analogues Hydroxyephedrine (HED) and Metaiodobenzylguanidine (MIBG) in Rat Hearts. *Eur. J. Nucl. Med. Mol. Imaging* **2013**, *40* (7), 1077–1083. https://doi.org/10.1007/s00259-013-2393-z.

(51) Higuchi, T.; Yousefi, B. H.; Kaiser, F.; Gärtner, F.; Rischpler, C.; Reder, S.; Yu, M.; Robinson, S.; Schwaiger, M.; Nekolla, S. G. Assessment of the ^{18}F-Labeled PET Tracer LMI1195 for Imaging Norepinephrine Handling in Rat Hearts. *J. Nucl. Med.* **2013**, *54* (7), 1142–1146. https://doi.org/10.2967/jnumed.112.104232.

(52) Yu, M.; Bozek, J.; Kagan, M.; Guaraldi, M.; Silva, P.; Azure, M.; Onthank, D.; Robinson, S. P. Cardiac Retention of PET Neuronal Imaging Agent LMI1195 in Different Species: Impact of Norepinephrine Uptake-1 and -2 Transporters. *Nucl. Med. Biol.* **2013**, *40* (5), 682–688. https://doi.org/10.1016/j.nucmedbio.2013.03.003.

(53) Werner, R. A.; Rischpler, C.; Onthank, D.; Lapa, C.; Robinson, S.; Samnick, S.; Javadi, M.; Schwaiger, M.; Nekolla, S. G.; Higuchi, T. Retention Kinetics of the ^{18}F-Labeled

Sympathetic Nerve PET Tracer LMI1195: Comparison with ^{11}C-Hydroxyephedrine and ^{123}I-MIBG. *J. Nucl. Med.* **2015**, *56* (9), 1429–1433. https://doi.org/10.2967/jnumed.115.158493.